Leadership in Sustainable Infrastructure
Leadership en Infrastructures Durables

Vancouver, Canada
May 31 – June 3, 2017/ *Mai 31 – Juin 3, 2017*

MODELLING ICE DYNAMICS IN THE UPPER SAGUENAY FJORD

A. Cornett [1,5], D. Watson [2], H. Babaei [3], M. Sayed [4]
[1, 2, 3, 4] National Research Council, Ottawa, Ontario, Canada
[5] Andrew.Cornett@nrc-cnrc.gc.ca

ABSTRACT

A numerical model of ice dynamics developed at the National Research Council of Canada has been set-up and applied to predict the dynamics of the ice cover in the upper Saguenay Fjord subject to forcing by ground level winds and near surface water currents. The model has been used to predict the evolution of ice pressure, ice concentration and ice thickness at sites being considered for development of new port facilities. Predictions for eleven different hypothetical scenarios were produced, each corresponding to a different combination of wind speed and direction, tide, freshwater inflow, initial ice thickness, and initial ice concentration. The scenarios include both extreme conditions with very low probability of occurrence, as well as more common conditions. The set-up and application of the ice dynamics model as well as the sensitivity of the predicted ice cover dynamics to variations in initial ice concentration, initial ice thickness, wind direction and wind speed is described and discussed.

Keywords: Saguenay Fjord, ice dynamics, ice pressure, ice thickness, ice concentration, numerical model

1. INTRODUCTION

The Saguenay Fjord extends for 110 km between the communities of Chicoutimi, where the fjord transitions to the Saguenay River, and Tadoussac, where the fjord meets the St Lawrence Estuary, see Figure 1. The Saguenay Fjord is notable for its complex and strongly stratified flows, with freshwater at the surface flowing over denser seawater at lower depths. During winter a stable ice cover forms over the upper part of the fjord, and commercial ships accessing port facilities in Chicoutimi and Port Alfred are escorted by ice breaking vessels operated by the Canadian Coast Guard. Ice breaking vessels are normally deployed before mid-March to initiate the Spring break-up and assist with ice clearing operations.

Figure 1. Map of the Saguenay Fjord region (source: Google).

A numerical model of ice dynamics previously developed at the National Research Council Canada has been setup and applied to support the planning of future port facilities in the upper part of the fjord. The model predicts the deformation of an ice cover over time and space due to forcing by wind and surface current. The wind and current forcing can be steady and uniform or unsteady and spatially varying. Initial conditions are specified by prescribing the initial ice concentration and initial ice thickness throughout the computational domain. Since the horizontal length scales of interest are much larger than the ice thickness, a depth-averaged formulation is employed, whereby the stresses and velocities are averaged over ice thickness. A parameterization of ice thickness redistribution is introduced in order to relate ridge (and ice rubble) formation and lead opening to the strain rates. Thus, the numerical solution keeps track of the evolution of deformed ice thickness and ridging. Further details on the ice dynamics model are given in Sayed *et al.* (2002) and Kubat *et al.* (2011, 2015).

In this study the ice dynamics model was used to predict the temporal and spatial evolution of ice concentration, ice thickness and ice pressure throughout the region for various hypothetical scenarios, each comprised of an initial ice condition combined with different wind and current forcings. The current forcing was obtained from a 3D numerical model of stratified hydrodynamics in the fjord, while the wind forcing was either derived from analysis of historical wind measurements or obtained from a numerical wind model.

Review and Characterization of Ice Conditions

A brief review of available information on ice conditions in the upper Saguenay Fjord was undertaken to characterize the range of local ice conditions and inform the ice dynamics modelling. Useful information was found in a report by Arctec Canada Ltd. (ACL, 1980) and in Urgales *et al.* (2002), Bourgault *et al.* (2011), and De Vernal *et al.* (2011).

Landsat satellite images for the period of 1972-2016, accessed through U.S. Geological Survey (USGS) online repository, were reviewed. Two examples showing the dramatic difference in the extent of the ice cover before and after the spring break-up are presented in Figure 2. The narrow shipping routes cleared by ice breaking vessels leading to/from two existing port facilities can be seen in Figure 2a.

Ice observation charts published by the Canadian Ice Service (CIS) were also obtained and reviewed. Two examples showing conditions in mid-March are shown in Figure 3. Various sub-regions are defined, each designated by a unique letter (A, B, etc.), and the concentration, stage of development (age) and form (floe size) of the ice in each sub-region is specified through a corresponding Egg code. Further guidance on interpreting ice charts can be found on the Canadian Ice Service website.

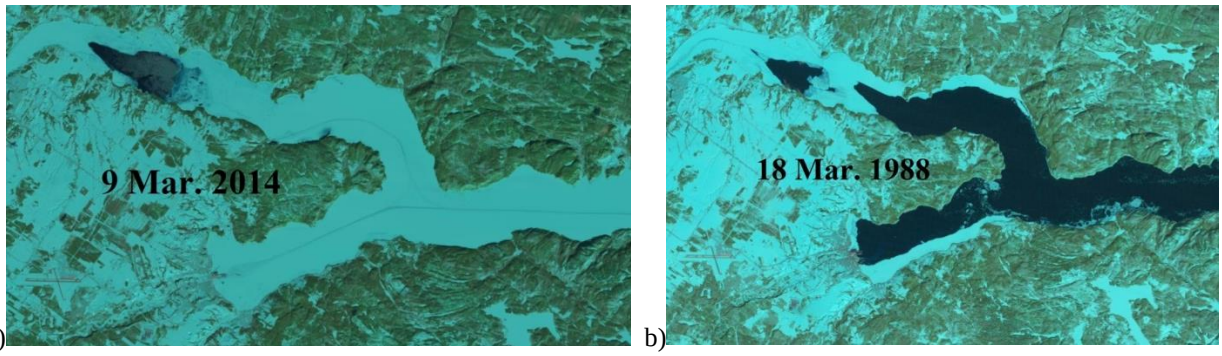

a) b)

Figure 2. Landsat images showing typical ice cover (a) before and (b) after Spring Breakup.

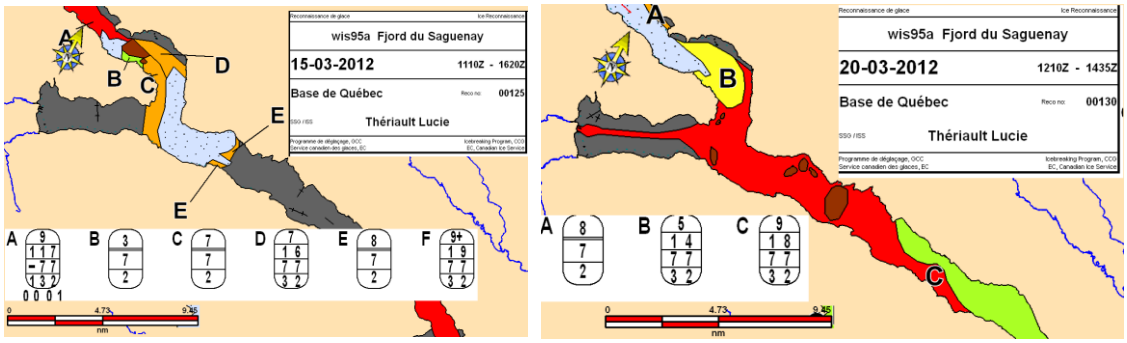

Figure 3. CIS ice charts showing ice conditions during mid-March.

Data on ice thickness acquired under the Ice Thickness Collection Program run from 1947-2002 by Environment Canada was also obtained and analyzed. Two hundred nine historical ice thickness measurements from three sites in the upper fjord are plotted in Figure 4a, while Figure 4b shows two exceedance probability curves derived from the data. Considering only observed seasonal maximums, the median thickness is 48 cm while the maximum is 70 cm. It is noted that thicker ice may well have occurred over the period but was not measured.

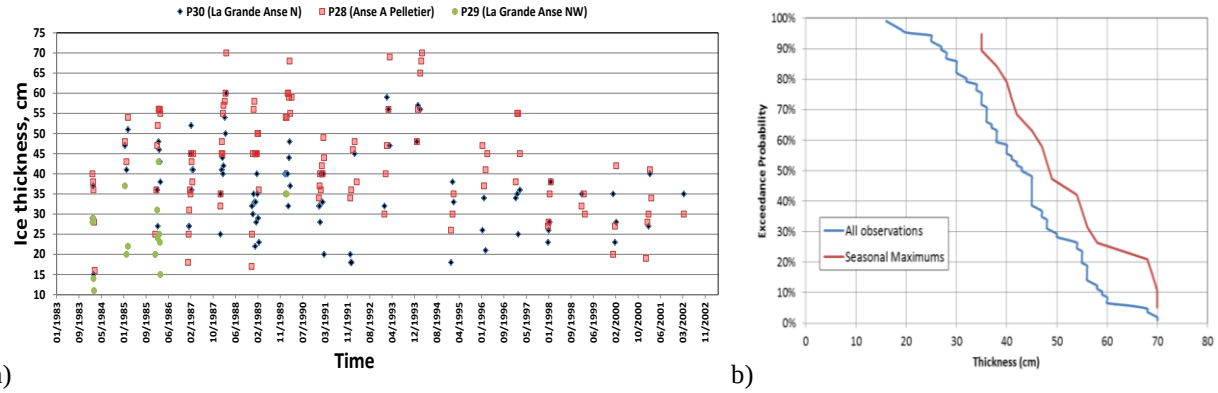

a) b)

Figure 4. Ice thickness data measured in the upper fjord from 1984 – 2002.

Following Gosink *et al.* (1986) thermodynamic thickness growth of ice sheets can be estimated by:

[1] $h = 3.5\times10^{-2}\times CFDD^{0.5}\times\alpha$

in which *h* and *CFDD* denote ice thickness in meters and cumulative freezing degree days in degrees Celsius (°C). The coefficient α, a positive number less than 1, depends mainly on local wind and snow conditions. Although this equation was originally developed to estimate ice thickness growth for lakes, it is thought to be applicable to streams when current speeds are smaller than approximately 0.6 m/s, which is the case for a large part of the upper Saguenay Fjord. Using some of the observed ice thickness values in Figure 4 for calibration yields a best fit value of $\alpha = 0.503$. Consideration of temperature records recorded at the Bagotville airport over the period from 1950 to 2015

yields a peak seasonal value of *CFDD* = 1,833 °C (for the 1958-1959 season). With this peak *CFDD* and assuming $\alpha = 0.503$ in Equation 1, a maximum ice thickness of 0.75 m can be estimated over the 65 year period.

Hydrodynamic Conditions

Detailed information on near surface currents throughout the upper fjord was required to force the ice dynamics model. As noted previously, the Saguenay Fjord is notable for its complex and strongly stratified flows, with freshwater at the surface flowing over denser seawater at lower depths. Moreover, the hydrodynamics are sensitive to the tide range and phase (ebb or flood) as well as the freshwater discharge entering the upper fjord from the Saguenay River.

The tides throughout the fjord are semi-diurnal, rising and falling twice daily. The tide range at Tadoussac, located near the mouth of the fjord, varies from ~2 m during Neap tides up to ~6 m during Spring tides. Typical tide ranges at Port Alfred, located in the upper fjord, are slightly higher, fluctuating from ~2.5 m up to ~6.5 m.

Data on the Saguenay River discharge at Shipshaw for the period 1972 - 2012 was obtained and analyzed. Based on this data, the average freshwater inflow is 1,310 m^3/s, while the inflow exceeded 1% of the time is 6,493 m^3/s. The inflow during the month of March when the ice-cover breaks up was also investigated. The mean inflow during March was found to be 1,244 m^3/s, while the maximum recorded inflow during March is 1,907 m^3/s.

A three-dimensional hydrodynamics model based on the Telemac-3D solver was set up to simulate the stratified hydrodynamics throughout the fjord. Open water conditions (without ice cover) were assumed for all of the hydrodynamic simulations. Further information on the development, calibration and application of the 3D hydrodynamics model together with a discussion of the simulation results is given in Cornett *et al.* (2017). Figure 5 shows the modelled distribution of near-surface current speed and direction across the upper fjord for one time step.

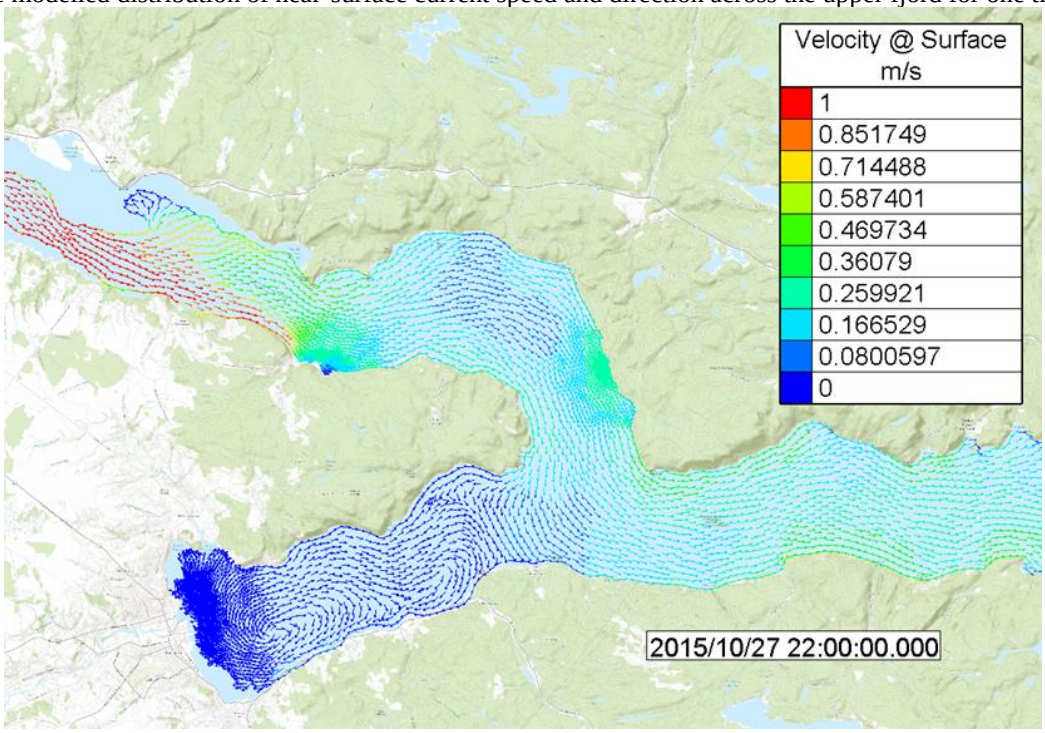

Figure 5. Modelled distribution of near surface current speed and direction for one time step.

Wind Conditions

Information on ground level winds in the region was also required to force the ice dynamics model. Two approaches were used to obtain this information: a) review and analysis of historical wind data recorded at Bagotville airport and several other sites in the region; and b) numerical simulation of wind fields.

Summary wind statistics derived from the Bagotville airport data are presented in Table 1. The two most common wind directions are west followed by east, while the strongest winds tend to approach from the west, north-west and east directions.

The Anemoscope wind simulation model, described in NRC (2006), was used to estimate the spatial distribution of ground level wind (speed and direction) for 16 extreme wind scenarios or atmospheric states. Anemoscope embodies the WEST wind mapping system described in Pinard *et al.* (2005) and Yu *et al.* (2006). Results for one such simulation are presented in Figure 6, for the case of an extreme wind approaching from ESE.

Table 1. Summary wind statistics (occurrence frequency in %) for Bagotville Airport (source: Environment Canada).

		Direction								
		NE	**E**	**SE**	**S**	**SW**	**W**	**NW**	**N**	**All**
Speed in km/hr	**< 1**									8.9
	1-10	1.6	8.4	4.7	3.2	3.9	7.0	2.6	1.3	32.6
	11-20	0.5	10.2	1.4	0.6	2.7	14.2	4.1	0.4	34.2
	21-30	0.1	5.3	0.4	0.1	0.9	7.7	2.5	0.1	17.1
	31-40	0.0	1.5	0.1	0.0	0.2	3.0	0.9	0.0	5.6
	41+	0.0	0.2	0.0	0.0	0.0	1.1	0.2	0.0	1.5
	All	2.2	25.6	6.6	3.9	7.6	32.9	10.4	1.8	100.0
	Avg. speed	9.0	15.7	9.0	7.6	12.1	18.6	17.9	8.8	14.2

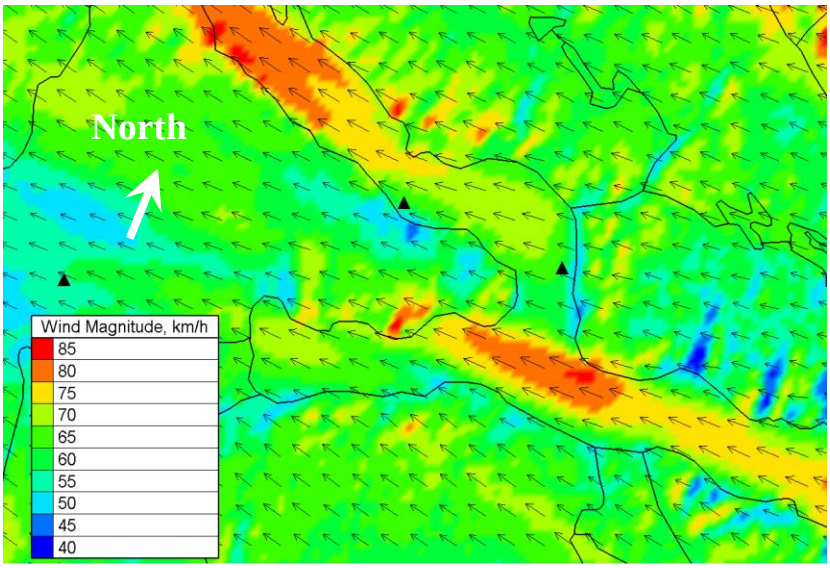

Figure 6. Modelled distribution of near ground wind speed and direction, extreme wind from ESE.

2. SCENARIO DEFINITION

An ice dynamics model previously developed at NRC was applied to investigate ice dynamics in the upper fjord for eleven hypothetical scenarios. The environmental and initial conditions for each scenario are summarized below in Table 2. All eleven scenarios assume a Spring (large) tide and begin when the initial water level in the upper fjord is high. Hence, the water level falls during the first 6 hours of each simulation, it then rises between the 6th and 12th hours. The narrow ice-free shipping corridors evident in Figure 2a were included in the initial condition for all scenarios.

Scenarios 1 to 4 have a high freshwater inflow of 1,907 m^3/s with an initial ice thickness of 70 cm and an initial ice concentration of 95%. The 1,907 m^3/s inflow is the maximum freshwater inflow recorded during the month of March. Scenario 1 has no wind (zero speed) while Scenarios 2 to 4 use spatially varying wind fields calculated by AnemoScope (example in Figure 6). It is worth noting that the extreme winds were sustained and held constant for the full duration of each ice dynamics simulation, typically six hours or more. While it is acknowledged that this represents an unrealistic scenario, the effect of extreme winds acting for shorter durations can be observed by examining intermediary simulation outputs (i.e. outputs after one hour).

Scenarios 5 to 11 all assume a freshwater inflow of 1,244 m^3/s, corresponding to the average freshwater inflow to the upper fjord during March, when the Spring break-up occurs. Initial ice thickness is either 43 cm (the average ice thickness reported in measurements taken over 18 seasons) or 70 cm (close to the thickest ice observed over 18 seasons). Initial ice concentration is either 95%, representing a full and virtually complete ice cover – i.e. stable conditions before the start of Spring break-up, or 70%, representing a situation with ice floes of various sizes and 30% open water. At the start of each simulation, both the ice thickness and ice concentration were assumed to be evenly distributed across the non-land portion of the computational domain, except for the narrow shipping corridors, where open water was assumed.

The initial distribution of ice thickness and ice concentration for Scenario 6 are shown in Figure 7. In this figure and other similar ones to follow, six different colours are used to denote ice concentration over the range from < 1/10 (low) to > 9/10 (high). Similarly, ice thickness variations over the range from < 20 cm to > 100 cm are denoted using six different colours. In both figures, warm colours denote more adverse ice conditions (thicker ice or higher concentrations) while colder colours denote more benign ice conditions. Conventional black wind barb symbols are used to denote the wind speed and direction, while small black vectors are used to indicate the water current speed and direction.

The 260° (from the west) wind direction modelled in Scenarios 5 to 8 is approximately shore normal to the eastern shore (labelled in Figure 7). Two wind speeds were modelled for this direction: 19 km/hr and 35 km/hr. The 19 km/hr wind corresponds to the average speed of the westerly winds (based on observed wind statistics at Bagotville), while the 35 km/hr speed is a more extreme condition that occurs less frequently. Again, it is worth noting that the winds were held constant for the full duration of each simulation.

The 22.5° (NNE) wind direction modelled in Scenarios 9 to 11 is approximately shore normal to the southern shore (labelled in Figure 7). Two wind speeds are modelled for this direction: 9 km/hr and 25 km/hr. The 9 km/hr speed is the average speed of the winds from NNE (based on observed wind statistics at Bagotville), while the 25 km/hr speed is a more extreme condition that occurs less frequently. These winds were sustained for the full duration of each simulation.

Table 2. Summary of initial ice conditions and environmental conditions for Scenarios 1 – 11.

Scenario	Tide range	Initial water level	Freshwater inflow (cms)	Current field	Wind speed @ Bagotville (km/hr)	Wind direction (deg N)	Wind field	Initial ice concentration (%)	Intial ice thickness (cm)
1	Spring	High	1907	Spatially and time varying	0	-	Spatially varying	95	70
2	Spring	High	1907	Spatially and time varying	80 [1]	262 (W)[1]	Spatially varying	95	70
3	Spring	High	1907	Spatially and time varying	53 [2]	30 (NNE)[2]	Spatially varying	95	70
4	Spring	High	1907	Spatially and time varying	61 [3]	90 (E)[3]	Spatially varying	95	70
5	Spring	High	1244	Spatially and time varying	19	260 (W)	Spatially uniform	95	43
6	Spring	High	1244	Spatially and time varying	35	260 (W)	Spatially uniform	95	43
7	Spring	High	1244	Spatially and time varying	35	260 (W)	Spatially uniform	95	70
8	Spring	High	1244	Spatially and time varying	35	260 (W)	Spatially uniform	70	43
9	Spring	High	1244	Spatially and time varying	9	22.5 (NNE)	Spatially uniform	95	43
10	Spring	High	1244	Spatially and time varying	25	22.5 (NNE)	Spatially uniform	95	43
11	Spring	High	1244	Spatially and time varying	25	22.5 (NNE)	Spatially uniform	70	43

1 Wind field derived from Climate State ANU1D293C14M (AnemoScope Simulation)
2 Wind field derived from Climate State ANU1D068C14M (AnemoScope Simulation)
3 Wind field derived from Climate State ANU1D135C14M (AnemoScope Simulation)

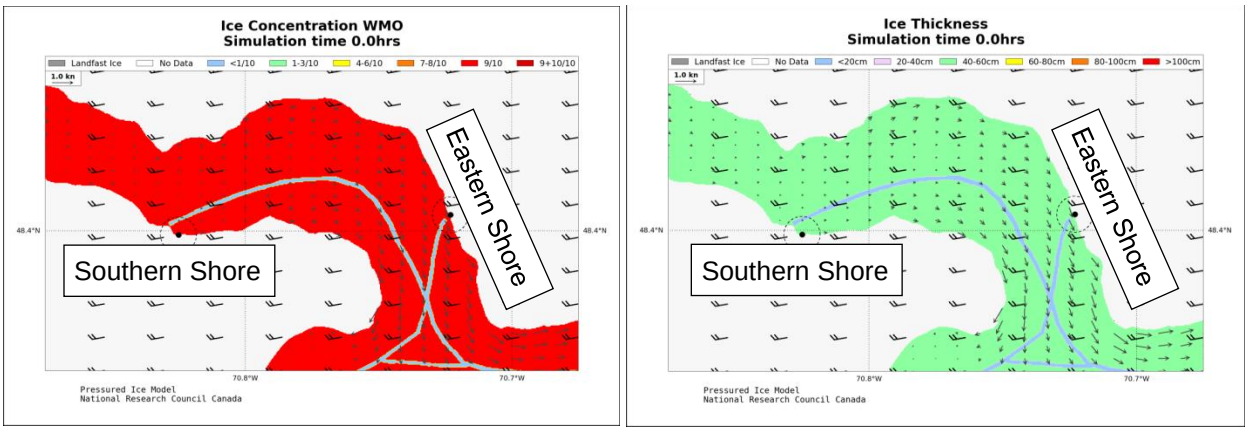

Figure 7. Initial distribution of ice concentration and ice thickness for Scenario 6.

3. ICE DYNAMICS MODEL SET UP

A rectangular computational grid extending 15 km in the east-west direction by 9 km in the north-south direction was set up to cover the region of interest, see Figure 8. The grid cell size chosen was 25 meters which is required to properly model the ice-free corridors that are roughly 125 m wide. The final grid is composed of 600 cells in the east-west direction and 360 cells in the south-north direction.

The ice dynamics model was forced using both ground-level wind and surface water current prescribed across the computational domain. A simple approach with no active coupling between the hydrodynamics and ice dynamics was followed in this study. The influence of the hydrodynamics on the ice cover was modelled, but the effect of the ice cover on the hydrodynamics was neglected. Similarly, the influence of the wind on the ice cover was modelled, but the effect of the ice cover on the wind (expected to be small) was neglected.

Numerical predictions of surface water currents that varied over both space and time were extracted from the output files of 3D hydrodynamic simulations that had been pre-computed (example in Figure 5). The water current was specified on an unstructured triangular grid, and linear interpolation was used to obtain the water current speed and direction for each cell of the ice dynamics grid at every time step. It is acknowledged that open water conditions (without ice cover) were assumed in the hydrodynamic simulations, hence the influence of the ice cover on the hydrodynamics was neglected. There is no doubt that this simplification introduces some uncertainly into the final results.

Only steady wind fields (that do not vary with time) were considered in this study, and in all cases the wind was assumed to remain steady throughout the ice dynamics simulation. For the cases where spatially varying ground-level wind fields were computed using the Anemoscope wind model, linear interpolation was used to obtain wind speed and direction at each cell of the ice dynamics grid. For other cases where spatially uniform ground-level winds were assumed, a uniform wind speed and direction was applied at each grid cell.

Test simulations were carried out to ensure that the model set-up could appropriately simulate the ice dynamics over the area of interest. The grid extent, grid cell size and simulation time step were all varied until stable simulation outputs were achieved. The final computational time step for the ice dynamics model was 5 s, the hydrodynamic forcing was updated every 30 minutes, and model outputs were stored every 15 minutes.

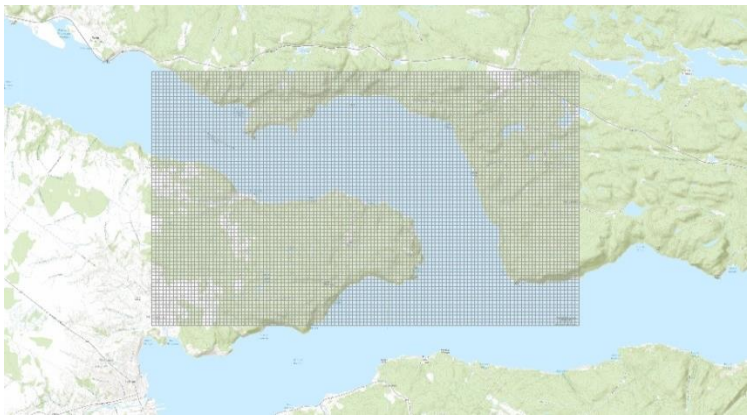

Figure 8. 15 km x 9 km ice dynamics model grid with 25 m x 25 m resolution.

4. RESULTS AND DISCUSSION

Each simulation predicts the evolution of the distributions of ice thickness, ice concentration and the stresses (or pressure) within the ice cover for the prescribed initial conditions and environmental forcing. We note that the pressure values resulting from the present simulations correspond to compaction and deformation processes that take place along length scales of 100s of meters. While they are indicative of the severity of ice conditions that may be manifested in ridging, rafting and pile-up of ice, they should not be used to estimate ice forces on a wharf or a vessel. The ice pressure can be characterized in terms of relative severity as *no pressure* (< 6 kN/m), *light* (6 to12 kN/m), *moderate* (12 to 24 kN/m), *strong* (24 to 40 kN/m) or *very strong* (> 40 kN/m), where ice pressure is expressed as a force per unit width. These pressure values are based on experience with the effect of pressure levels on the ability of vessels to navigate through an ice cover (Kubat *et al.*, 2015).

We present here in some detail the results for two scenarios. One of these (Scenario 6) produces pronounced ice action against the eastern shore, where construction of a new wharf is being considered. The other (Scenario 10) produces ice action against the southern shore where port facilities are currently located.

The initial evolution of ice pressure over the first hour of Scenario 6 is illustrated in Figure 9. In this scenario an ice cover with an initial uniform thickness of 43 cm, and uniform concentration of 95% is subject to a 35 km/hr wind approaching from west. The hydrodynamic conditions correspond to a falling Spring tide during March. For these conditions, the ice dynamics are dominated by the 35 km/hr wind from the west, which is sufficient to mobilize the ice cover, which deforms and compacts against the eastern shore. Under these strong winds, the effects of hydrodynamic forcing on the ice cover are relatively minor compared to the wind stress. The ice-free channels close early in the simulation as the wind pushes the ice eastwards. The ice cover deforms progressively over the first five hours until reaching a near steady state condition thereafter. The modelled distributions of ice concentration, thickness and pressure after five hours are shown in Figure 10. These results show that the ice conditions along the eastern shore become relatively severe, with concentration reaching 100% and thickness reaching up to 80 cm (initially 43 cm) combined with strong pressure. While ice conditions along the eastern shore worsen, the western and southern parts of the domain become largely free of ice.

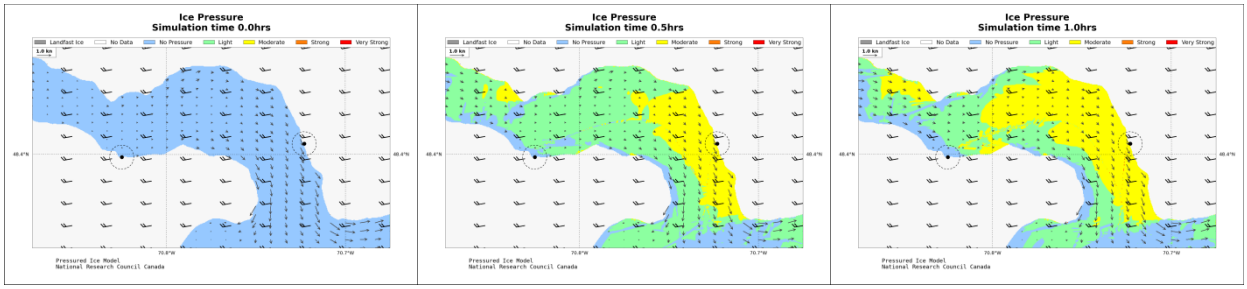

Figure 9. Initial evolution of ice pressure severity for Scenario 6 (35 km/hr wind from west).

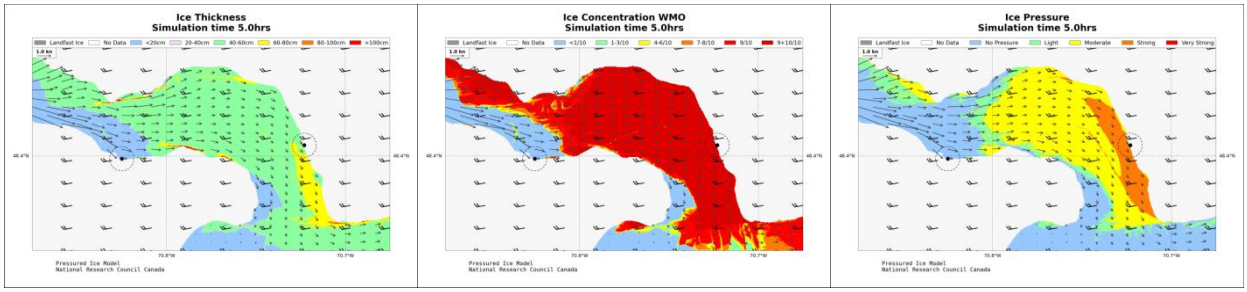

Figure 10. Distribution of ice cover thickness, concentration and pressure after 5 hours for Scenario 6.

In Scenario 10, the same initial ice cover considered in Scenario 6 is exposed to the same hydrodynamic forcing, this time combined with a 25 km/h wind approaching from the north-northeast direction. The initial evolution of ice pressure for this case is illustrated in Figure 11, while the distributions of ice thickness, concentration and pressure after 5 hours are shown in Figure 12. For these conditions the ice dynamics is again dominated by the wind forcing: the ice cover rapidly deforms and compacts against the southern shore in response to the wind stress. The ice cover deforms progressively over the first ~5 hours, becoming nearly stable thereafter. The simulation results indicate that the ice conditions along the southern shore grow increasingly severe, with concentration reaching 100% and thickness exceeding 80 cm (initially 43 cm) combined with strong to very strong pressure. In contrast, the northern and eastern shores become largely ice free.

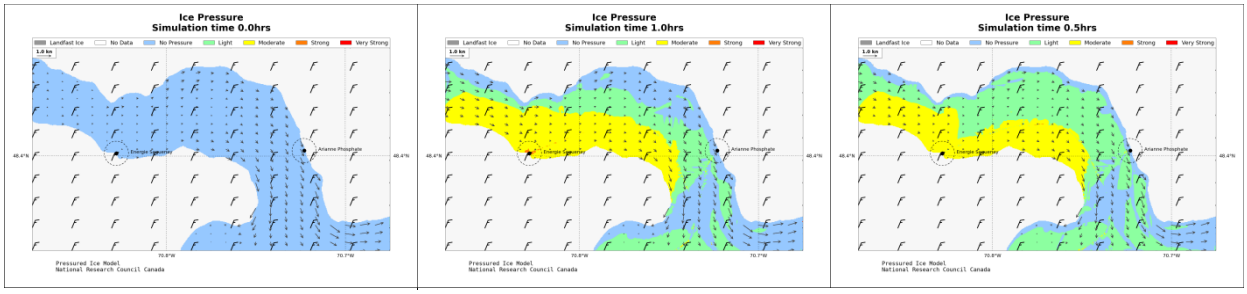

Figure 11. Initial evolution of ice pressure severity for Scenario 10 (25 km/hr wind from north-northeast).

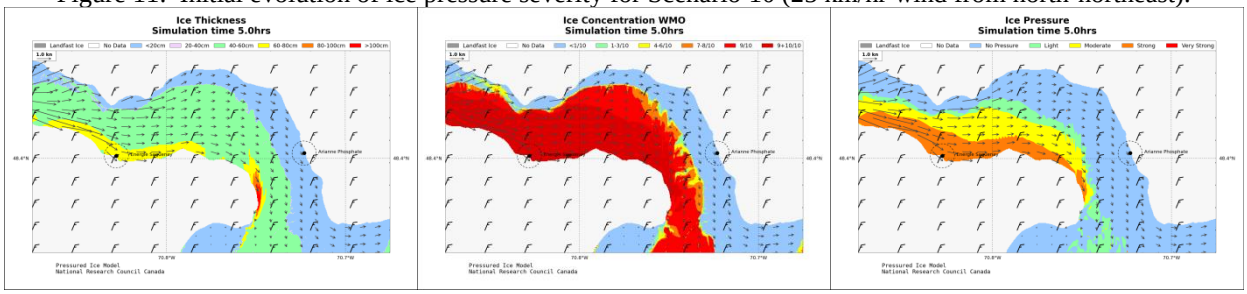

Figure 12. Distribution of ice cover thickness, concentration and pressure after 5 hours for Scenario 10.

The average ice thickness and average ice pressure forecast at the 5 hr mark of each scenario is presented graphically in Figure 13 for two locations, one near the center of the Southern shore and the other near the center of the Eastern shore. According to the simulation results, Scenarios 5 to 8, which all consider wind from the west, produce moderate to severe ice conditions along the eastern shore. The severity of ice conditions in this location is greatest for scenario 7 in which relatively thick 70 cm ice is modelled together with a relatively strong 35 km/hr wind. Thicker ice and/or stronger winds produce more severe ice conditions, as expected. For Scenario 8, which combines average ice thickness (43 cm) with reduced initial ice concentration (70%), the build-up of ice pressure is delayed in comparison with scenarios 5 to 7 in which higher initial ice concentration (95%) was modelled. Thus, the build-up of pressure along the eastern shore after a specific intermediate duration, say 3 hours, is significantly reduced for Scenario 8 compared to the others. However, the peak pressure reached at the end of the simulation (12 hours) remains similar, it just takes longer for the pressure in the ice cover to reach these levels when the initial concentration is lower.

Winds from the north-northeast were modelled in Scenarios 9 – 11, resulting in appreciable ice action against the southern shore. The ice build-up along the southern shore was most severe for Scenario 10 (stronger wind combined with high initial ice concentration) and least severe for Scenario 11 (stronger wind combined with lower initial ice concentration). Results for Scenario 9 (weaker wind combined with high initial ice concentration) indicate a medium ice severity when compared against the other two cases. The build-up of ice pressure against the southern shore occurred much more slowly in Scenario 11, when a lower initial ice concentration was modelled.

It should be mentioned that the results of this study should be associated with a moderate degree of uncertainty due to the many assumptions, simplifications and limitations inherent in the methodology followed to obtain them. Despite this important caveat, the simulation results show that wind conditions are the primary factor in mobilizing and deforming the ice cover leading to moderate or severe ice conditions along the shore of the upper Saguenay Fjord. Moderate and strong sustained winds acting against either shoreline can be expected to increase the severity of ice conditions. In contrast to wind action, water currents appear to play a minor role in the ice dynamics for this region. This conclusion is corroborated by the results of Scenario 1, in which wind forcing was excluded (calm conditions). Only the time-varying water current acted on the ice cover in Scenario 1. Simulation outputs for this scenario indicate that the ice cover remains stationary with no detectable movement; the navigation channels remain intact and ice-free, and the ice pressures in the ice cover remain light throughout the region.

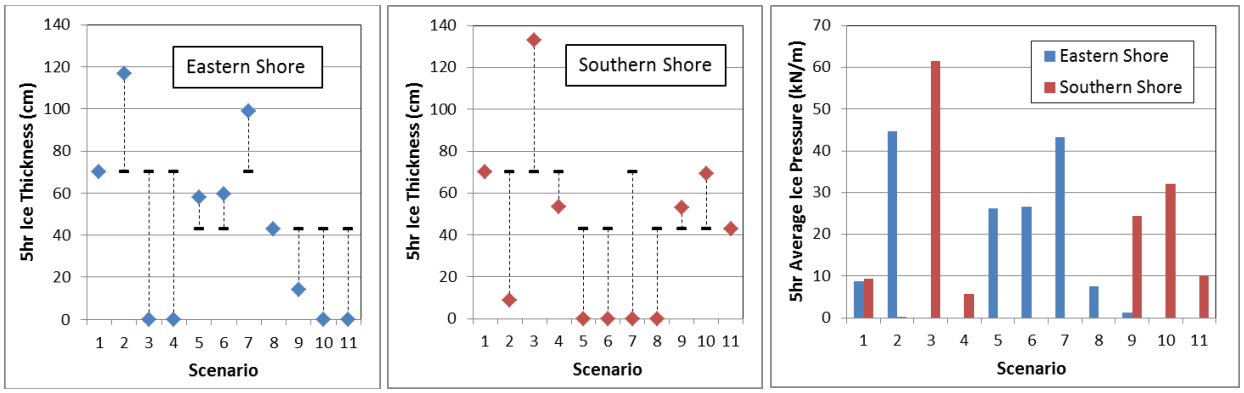

Figure 13. Average Ice thickness and pressure near Southern and Eastern shores for Scenarios 1-11, after 5 hours.

5. CONCLUSION

A numerical model of ice dynamics previously developed at the National Research Council Canada has been setup and applied to support the planning of future port facilities in the upper part of the fjord. The ice dynamics model has been used to predict the evolution of ice pressure, ice concentration and ice thickness in response to forcing by ground level winds and surface water currents. The hydrodynamic forcing was obtained from a newly developed 3D numerical model of stratified hydrodynamics in the fjord, while the wind forcing was either derived from analysis of historical wind measurements or obtained from a numerical wind model. Results for eleven hypothetical scenarios covering both non-extreme and extreme conditions have been obtained.

The simulation results suggest that, aside from the action of ice clearing ships, wind conditions are the primary factor in mobilizing and deforming the ice cover in the upper Saguenay Fjord. The hydrodynamic forcing is a secondary factor in comparison to the wind, due to the relatively low water current speeds that prevail over most of the study region. Moderate or severe sustained winds from northerly directions can mobilize the ice cover, which deforms and compacts as it moves southwards, creating moderate to severe ice conditions along the southern shore. Similarly, strong or extreme winds approaching from westerly directions are able to mobilize the ice cover, which deforms and compacts as it moves eastwards, creating moderate to severe ice conditions along the eastern shore. The numerical simulations suggest that the severity of the ice conditions along either shore intensify with increasing initial ice thickness and/or increasing wind speed. Lower wind speeds and/or thinner ice tend to produce more moderate near-shore ice conditions, as expected. Lower initial ice concentration tends to delay the build-up of ice pressure and thickness near both shores.

The NRC ice dynamics model is an important tool for forecasting ice conditions that may influence navigation safety, port operations and the development of new port facilities at higher latitudes where ice covered waters persist, such as the Saguenay Fjord.

6. REFERENCES

Arctec Canada Ltd. (ACL), 1980. *Ice Conditions at a Proposed Dock Site at Grande Anse, Saguenay River*. Report to the SNC Group.

Bourgault, D., Galbraith, P., Winkler, G., 2011. Exploratory Observations of Winter Oceanographic Conditions in the Saguenay Fjord. *J. ATMOSPHERE-OCEAN* 50 (1) 2012, 17–30.

Cornett, A., Pilechi, V., Cousineau, J., 2017. Modelling stratified hydrodynamics in the Saguenay Fjord with Telemac-3D. *Proc. 23rd Canadian Hydrotechnical Engineering Conf.*, CSCE, Vancouver, Canada.

De Vernal, A., St-Onge, G., Gilbert, D., 2011. Oceanography and Quaternary geology of the St. Lawrence Estuary and the Saguenay Fjord. *IOP Conf. Series: Earth and Environmental Science* 14 (2011).

Gosink, J., Marcotte, N., Muller, A., and Osterkamp, T.E., 1986. Thermal Regime of Lakes and Rivers: Chapter 4 of *River and Lake Ice Engineering*, Edited by Larsen P., Ashton, G., Water Resources Publications, Colorado.

Hervouet, J-M, 2007. *Hydrodynamics of Free Surface Flows: Modelling with the Finite Element Method*. Wiley Scientific. 360 p.

Kubat, I., Watson, D. and Sayed, M., 2011. Characterization of Pressured Ice Threat to Shipping, *Proc. 21st Int. Conf. on Port and Ocean Engineering under Arctic Conditions (POAC)*, 2011, Montreal, Canada, pp 11-136.

Kubat, I, Sayed, M., and Lamontagne, P., 2015. Analysis of vessel besetting over the Gulf of St. Lawrence and the Strait of Belle Isle, winter 2013-2014, *Proc. 23rd Int. Conf. on Ports and Ocean Engineering under Arctic Conditions (POAC)*, June 14-18, Trondheim, Norway.

National Research Council Canada (NRC), 2006. *AnemoScope© Reference Guide*. 55 pages.

Sayed, M., Carrieres, T., Tran, H. and Savage, S.B., 2002. Development of an operational ice dynamics model for the Canadian Ice Service. *Proc. 2002 Int. Offshore and Polar Eng. Conf., ISOPE*, Kitakyushu, Japan, pp 841-848.

Urgeles, R., Locat, J., Lee, H., Martin, F., 2002. The Saguenay Fjord, Quebec, Canada: Integrating marine geotechnical and geophysical data for spatial seismic slope stability and hazard assessment. J Marine Geology 185 (2002) 319-340.